



INNSPUB

RESEARCH PAPER

**Journal of Biodiversity and Environmental Sciences (JBES)**

ISSN: 2220-6663 (Print) 2222-3045 (Online)

Vol. 6, No. 4, p. 541-551, 2015

<http://www.innspub.net>**OPEN ACCESS**

## Preparation of nanospinel $\text{La}_{1-x}\text{Sr}_x\text{CrO}_3$ using hydrothermal method and their applications on removal of azo dye from aqueous solutions

Maryam Maskanati, Haman Tavakkoli\*

*Department of Chemistry, College of Science, Ahvaz Branch, Islamic Azad University, Ahvaz, Iran*

Article published on April 30, 2015

**Key words:** Nanopowder, Perovskite-type oxide, Hydrothermal method, Dye removal, Kinetic studies.

### Abstract

In The present study, nanoparticles of perovskite-type  $\text{La}_{1-x}\text{Sr}_x\text{CrO}_3$  (LSCO) were prepared by Hydrothermal method in the presence of NaOH as a chelating agent. A series of common analytical techniques were used to characterize of the nanopowders. Thermal decomposition process of the complex precursor was examined by means of thermal gravimetric analysis (TGA). The surface morphology and composition of these nanopowders were also investigated using scanning electron microscopy (SEM). X-ray diffraction (XRD) patterns showed that single perovskite phase has been completely formed after calcinations treatment and transmission electron microscopy (TEM). The average particle size of LSCO is about 30 nm. The Fourier transform infrared (FT-IR) spectra were also measured for studying of structure of prepared nanopowders. The nanoparticles showed the excellent adsorption properties towards Bromo thymol blue ( $\text{C}_{27}\text{H}_{28}\text{Br}_2\text{O}_5\text{S}$ ). The adsorption studies have been carried out at different pH values, initial dye concentration and adsorbent doses to the optimum conditions. the removal of BTB above 88% was achieved. The Kinetic studies indicate that the removal process obeys the second-order kinetic equation. Also, The experimental isotherms were analyzed with four parameters equations (Freundlich, Langmuir, Temkin, and Redlich–Peterson) using linear regression.

\*Corresponding Author: Haman Tavakkoli ✉ [htavakkoli59@gmail.com](mailto:htavakkoli59@gmail.com)

## Introduction

From the effluent of textile, paper, printing, and leather industries are the major sources of water contamination. The presence of dyes in water reduces light penetration and hinders photosynthesis in aquatic plants (Sloker *et al.*). Some dyes and their degradation products in surface water are reported to be highly carcinogenic (Brown *et al.*). It is, therefore, essential to treat the dye effluents prior to their discharge into the receiving water. Dyes are organic compounds consisting of two main groups of compounds, chromophores (responsible for color of the dye) and auxochromes (responsible for intensity of the color) (Christie *et al.*). Dyes are classified according to the chemical structure and type of application. Based on chromophores, 20–30 different groups of dyes can be discerned, with azo, anthraquinone, phthalocyanine and triarylmethane accounting for the most important groups. Azo (around 70%) and anthraquinone (around 15%) compose the largest classes of dyes. Many processes are employed to remove dye molecules from colored effluents; in general, treatment methods 1. Introduction growing concern for public health and environmental quality has prompted a wide interest in developing and implementing various materials and methods for removing the toxic organic and inorganic pollutants from water. Dyes can be divided into three categories: (i) physical methods such as adsorption (El Qada and Chatterjee *et al.*), and membrane filtration (Ahmad *et al.*); (ii) chemical methods such as ionic exchange (Labanda *et al.*), chemical oxidation (Xu and Bradu *et al.*), electrochemical degradation (Chen *et al.*), and ozonation (Nawrocki *et al.*); and (iii) biological degradation (Mezohegyi *et al.*). Adsorption techniques for wastewater treatment have become more popular in recent years because of their efficiency in the removal of pollutants which are stable in biological degradation process. Adsorption can produce high quality water while also being a process that is economically feasible (Choy *et al.*). The physical characteristics of the adsorbents, such as, surface area, porosity, size distribution, density and surface

charge have high influence in the adsorption process. As a result, there has been a great interest in developing new adsorbent materials with diverse compositions, properties and functionalities. The family of perovskite-type oxides generally formulated as  $ABO_3$  (A is a rare earth metal with large ionic radius or alkali earth metals; B is a transition metal with a small ionic radius) could be considered as an adsorbent/catalyst material for the removal of dyes (Jeong and Carbajo *et al.*). Though, several articles have investigated the effectiveness of spinel-type oxides as catalysts for photodegradation and removal of water-soluble dyes (Lou and Yazdanbakhsh *et al.*), to our knowledge, the confirmation and optimization of the efficiency of the perovskite oxides catalysts and the degradation pathway for the removal of azo dyes from aqueous solution have received little attention in the literature.

According to this point that dyes are carcinogenic and hazardous materials, the main goal of this work, is investigation of the efficiency of perovskite-type oxide nanoparticles,  $La_{1-x}Sr_xCrO_3$  (LSCO), as an adsorbent for removal of azo dye, Bromo thymol blue (BTB), from aqueous media. The effect of different variables including concentration of dye, different pH values, adsorbent doses and reaction time, for removal of BTB on LSCO nanopowders has been evaluated. Furthermore, fabrication of LSCO nanoparticles via hydrothermal method as a new approach is other important aspect of this study.

## Material and methods

### Synthesis procedure

The perovskite precursor in this work was prepared by the NaOH-based. Furthermore, preparation of LSCO nanoparticles via hydrothermal method and its characterization by different techniques such as modified pechini method. Reagents of  $La(NO_3)_3 \cdot 6H_2O$ ,  $Sr(NO_3)_2 \cdot 6H_2O$ ,  $Cr(NO_3)_2 \cdot 6H_2O$  and NaOH (0.1M), were used as starting materials. Then the aqueous solutions of metal nitrates with nominal atomic ratios La: Sr: Co = 0.5: 0.5: 1 (LSCO) were mixed together in deionized water. NaOH was

proportionally added to the metal solution to have the same amounts of equivalents. The  $\text{LaSrCrO}_3$  perovskite-type oxides were prepared by  $\text{NO}_3$  coprecipitation method involving calcination at  $700^\circ\text{C}$ . The hydrothermal treatment to the perovskite-type oxide with water under autogeneous pressure was carried out in a closed stainless steel bomb, using 1.6 ml water per gram of perovskite-type oxide, at one temperature for 48 h. The hydrothermal treatment to the  $\text{LaCoO}_3$  with steam at atmospheric pressure was carried out in a conventional quartz reactor by passing a mixture of steam and  $\text{N}_2$  (60 mole% steam) at a space velocity of  $5100 \text{ cm}^3\text{g}^{-1}\text{h}^{-1}$ . After the hydrothermal treatment, the perovskite-type oxides were calcined at  $700^\circ\text{C}$  for 2h.

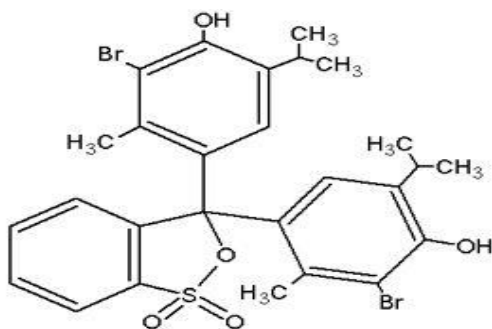


**Fig. 1.** Molecular structure of BTB dye.

#### Characterization

The decomposition and reaction processes of the dried polymeric gel have been analyzed by differential thermal analysis (DTA) and thermo gravimetric analysis (TGA) using a STA 503, Germany, in the temperature range from room temperature to  $1000^\circ\text{C}$ , in air with a heating rate of  $10^\circ\text{C}/\text{min}$ . The complex polymeric gel and derived powders have been also analyzed by Fourier transform infrared (FTIR) spectroscopy on Perkin Elmer BX II FTIR spectrometer. The crystallization and microstructure of the oxide powders have been characterized with an X-ray diffract meter employing a scanning rate of  $0.02 \text{ S}^{-1}$  in a  $2\theta$  range from  $20$  to  $80^\circ$ , using a  $\text{CuK}\alpha$  radiation. The data have been analyzed using JCPDS standards. The microstructure and elemental distribution on the surface were investigated using

KYKY EM 3200 ( $V=30\text{kV}$ ) scanning electron microscopy (SEM), and transmission electron microscopy (TEM) and energy dispersive X-ray spectroscopy (EDX, Inca 400, Oxford Instruments). A UV-Vis spectrophotometer (Perkin Elmer lambda 35) was employed to monitor adsorption of dye.

#### Dye removal test

A prepared solution of BTB was distributed into different flasks (50 ml capacity) and pH was adjusted with the help of the pH meter. The initial pH value of the dye solution was adjusted to the desired levels, using either HCl (0.5 M) or NaOH (0.5 M). A known mass of nano-LSCO powder (catalyst dosage) was then added to 10 mL of the BTB aqueous solution, and the obtained suspension was immediately stirred for a predefined time. All experiments were done at the room temperature. The investigated ranges of the experimental variables were as follows: dye concentration (100-300 mg/L), pH of solution (1-12), catalyst dosage (0.005, 0.01 and 0.02) and mixing time (1-30 min). The concentration of the dye in the reaction mixture at different reaction time was monitored by spectrophotometry by measuring the absorption intensity at  $\lambda_{\text{max}} = 432 \text{ nm}$  with a calibration curve. The removal efficiency of BTB was defined as follows (1):

$$\text{Removal rate \%} = \frac{C_o - C(t)}{C_o} \times 100 \quad (1)$$

Where  $C_o$  is the initial concentration of BTB and  $C_i$  is the concentration of BTB at certain reaction time  $t$  (min).

## Results and discussion

#### Thermal analysis

Differential thermal analysis (DTA) of the dried precipitate was recorded simultaneously on an apparatus manufactured by STA 503 (Germany). The DTA curve of LSCO was shown in Fig. 2. According to this curve the endothermic peak at  $131^\circ\text{C}$  can be attributed to the decomposition of the calcium citrate into its oxide. The second endothermic peak at  $320^\circ\text{C}$  can be attributed to the decomposition of the cobalt

citrate into its oxide. The third endothermic peak at 558 °C on this curve may be due to the formation of lanthanum oxide.

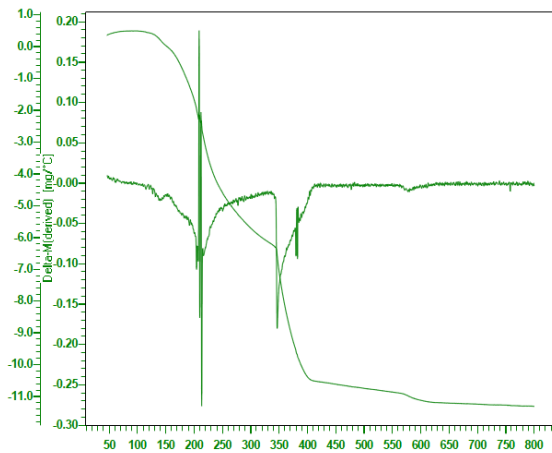


**Fig. 2.** DTA curve of the LSCO precursors obtained by Hydrothermal method.

Fig. 3 show TGA curves of the thermal decomposition process of LSCO xerogel obtained at a heating rate of 10°C/min in the air from room temperature to 800°C. The total weight loss of the xerogel was approximately 62% and the decomposition process can be divided into two distinct steps. The first weight loss occurs during the heating step from 50°C to 290°C (32%), which is due to the dehydration and decomposition of nitrates. In this area, DTA curve shows an exothermic peak at 130°C.

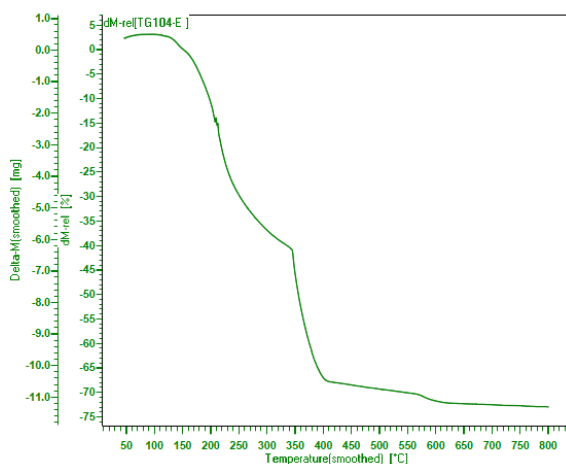


**Fig. 3.** TGA/DTG curves of the LSCO xerogel carried out from room temperature to 1000°C in air.

A weight loss of about 30% is observed from 290°C to around 560°C, which corresponds to the oxidizing combustion of the organic compounds such as citric acid (forming carbonate and oxide with cation). The DTA curve reveals a strong exothermic peak at 330°C which is likely due to the oxidation or combustion of the chelate complex which happen along with forming the metal oxides. No obvious change was observed above 600°C. Hence, it is plausible to conclude that the optimum calcination temperature is about 650°C.

*X-ray structural analysis*

The XRD patterns for the heat treated LSCO powders are shown in Fig. 4. Samples were heat treated at 700°C for 9 h (heating rate: 3°C/min) after previously dwelling at 110°C for 18 h. The XRD results reveal the existence of a perovskite-type phase for hydrothermal method at this temperature. As Fig. 4 shows, La<sub>0.5</sub> Sr<sub>0.5</sub> CrO<sub>3</sub> exhibited a crystalline perovskite phase (ABO<sub>3</sub>) with relevant diffraction peaks properly indexed. In this pattern we can identify the presence of (2 1 0), (0 1 1), (4 0 1), (2 0 2) and (6 0 2) crystal planes of metallic hexagonal-rhombohedral structure for LSCO. At higher temperatures, an increase in the intensity of the crystalline diffraction lines is observed.

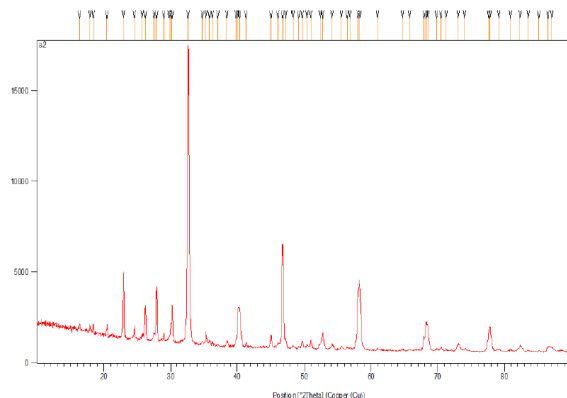


**Fig. 4.** XRD patterns of samples of the LSCO nanopowder calcinated at 650°C.

The crystallite grain size of the monophasic samples was determined from the full width at half-maximum width (FWHM) of the XRD (0 1 1) peak using the Scherer’s formula (2):

$$D_{hkl} = \frac{0.9\lambda}{\beta_{hkl} \cos \theta_{hkl}} \quad (2)$$

Where  $D_{hkl}$  is the particle grain size perpendicular to the normal line of (h k l) plane,  $\beta_{hkl}$  is the full width at half maximum,  $\theta_{hkl}$  is the Bragg angle of (h k l) peak, and  $\lambda$  is the wavelength of X-ray. The results indicate that LSCO nanopowders sizes calcinated at 650°C are ~ 15.75 nm.

#### SEM images analysis

The SEM analysis was carried out in order to determine the morphology of the sample. Fig.5 shows the micrograph of the samples synthesized by the hydrothermal method and calcinated at 700 °C. Based on the SEM images, porosity of the surface is evident and it seems that the particles have grown with uniform size. The size of pores varied from 22 to 40 nm. It must be mentioned that catalytic pores of large geometric dimension are more suitable for application to the adsorption process in liquid phase due to the simplicity and easiness in solid-liquid separation and thus with much improved workability for the catalysts. The surface looks scaly and nearly fully covered with the particles grown on it. Further, it can also be seen from the SEM image that in addition to the larger particles, the surface contains also rather smaller particles. However, appearance of bigger particles on the surface looks to be dominant. The aggregation of the smaller particles (in the nm range) may result in bigger LSCO NPs on the surface.

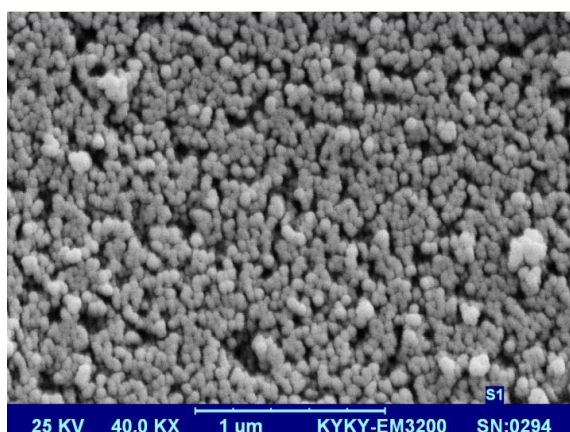


Fig. 5. SEM images of LSCO nanopowders.

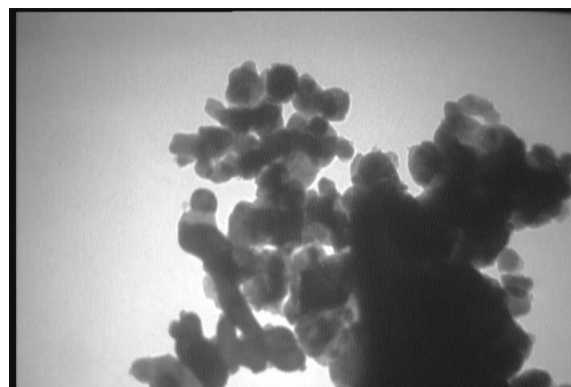


Fig. 6. FT-IR spectra of LSCO xerogel (a), and the calcinated powders at 700 °C (b).

#### IR spectra

Fourier transform infrared spectra were obtained for xerogels and nanopowder samples after heating treatment leading to the oxides. Figs. 7(a,b) show the FTIR spectra of the LSCO powders in the range of 600-4000  $\text{cm}^{-1}$ , calcined at 700°C and fresh xerogels. The FTIR spectrum is similar to the most other  $\text{ABO}_3$ -type perovskite compounds which have common  $\text{BO}_6$  oxygen-octahedral structure. Two samples show the typical M-O-C pair vibrations around 1636 and 1442  $\text{cm}^{-1}$ . The characteristic band at about 1254  $\text{cm}^{-1}$  corresponds to the anti-symmetric  $\text{NO}_3^-$  stretching vibration. A broad band is observed between 3400 and 3500  $\text{cm}^{-1}$  corresponds to the O-H stretching vibration due to water species occluded into the gel. The FTIR spectra of calcined sample shows the vanishing of bands related to organic and hydroxyl groups. Two bands are observed at 400-650  $\text{cm}^{-1}$  in the FTIR spectrum of sample, one of them is strong at ~ 617  $\text{cm}^{-1}$  and other weak peaks at 431  $\text{cm}^{-1}$ . These peaks are characteristics of perovskite oxides and can be attributed to  $\nu$  M-O stretching and  $\delta$  O-M-O bending mode of vibrations, respectively.

#### Adsorption study

##### Effect of pH

Solution pH is an important parameter that affects adsorption of dye molecules. The effect of the initial solution pH on the dye removal efficiency of BTB by LSCO particles was evaluated at different pH values, ranging from 1 to 12, with a stirring time of 15 min.

The initial concentrations of dye and adsorbent dosage were set at 50 mg/L and 0.01 g, respectively.

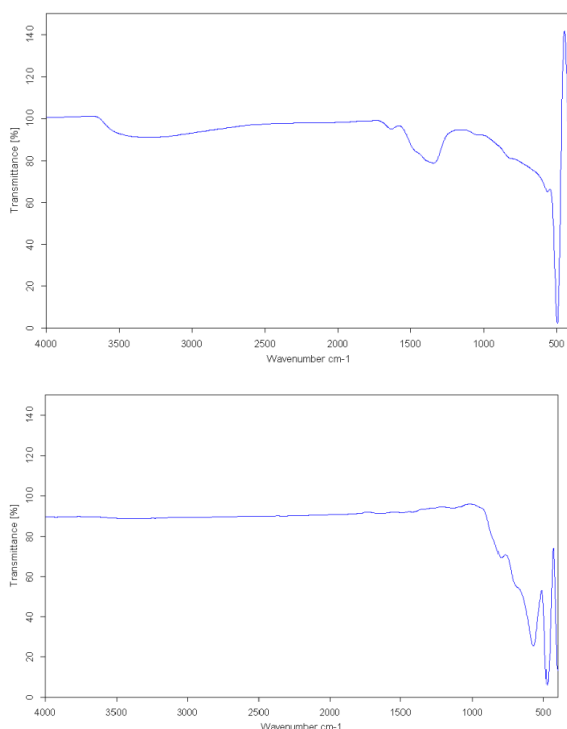


**Fig. 7.** Effect of initial pH of dye solution on removal of Eosin (LSCO dosage = 0.005 g, initial dye concentration = 100 mg/L, stirring time = 15 min).

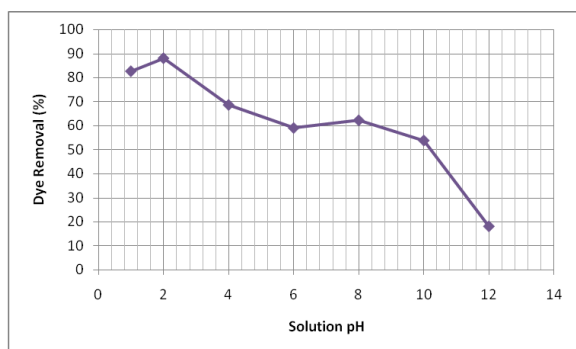


**Fig. 8.** Effect of stirring time on removal of EBT in different doses 0.007g, 0.005g, 0.01g, 0.02g of LSCO (initial dye concentration = 100 mg/L, initial pH 2).

As shown in Fig. 8, the dye removal was much higher in acidic pH (pH 1 and 2), and decreased when the pH was increased from 3 to 13. Since the removal of BTB increased to its maximum value at pH 2 (the removal of BTB above 88% was achieved) the electrostatic attraction between the dye molecules (negatively

charged) and LSCO surface (positively charged) might be the predominant adsorption mechanism. Therefore, to have the optimized condition to remove BTB, acidic pH should be applied and pH 2 seems to lead to the best result; so this pH was selected to run further experiments.

*Effect of contact time and adsorbent dosage*

To further assessing of dye removal, the effects of contact time and adsorbent concentration on the removal of BTB by LSCO nanoparticles were examined. Initial dye concentrations and pH of the solutions were fixed at 50 mg/L and 2, respectively, for all the batch experiments.

Results are shown in Fig. 9. As indicated, increasing of contact time in different dosages of adsorbent led to decrease in the concentration of BTB. This behavior was also observed when adsorbent dosage increased from 0.005 to 0.02 g. This decreasing in the concentration is due to the adsorption of BTB on LSCO nanoparticles and the greater number of adsorption sites for dye molecules made available at greater LSCO dosages.

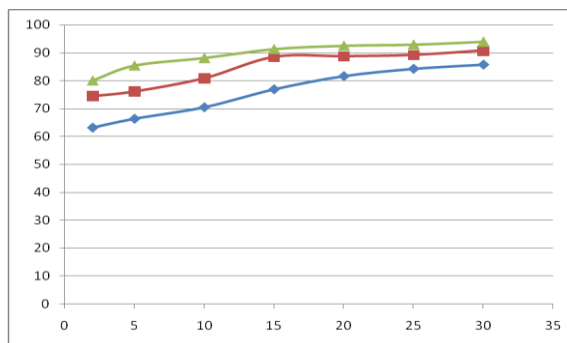


**Fig. 9.** Effect of initial dye concentration on removal of EBT (LSCO dosage = 0.005 g, initial pH = 2, stirring time = 15 min).

The removal efficiency of BTB at the initial dosage of 0.01 g, increased from 74% at the second minute of contact to 88% at time equals to 15 min by keeping constant stirring, however, with increasing LSCO dosage to 0.02 g the percentage of removal obtained in the second minute of stirring was 80%, and complete removal (90%) was attained when the stirring was

continued till time equals to 15 min. The low adsorbent dosage used for complete removal of BTB on to LSCO nanopowder is advantage of this study.

*Effect of dye concentration*

The initial dye concentration is another important variable that can affect the adsorption process. The effect of initial BTB concentration on dye removal efficiency by LSCO particles was studied by varying the initial dye concentration from 100 to 300 mg/L at pH=2, a adsorbent dosage of 0.01 g and contact time of 15 min, as shown in Fig. 10. Results show that decolorization of textile dye BTB decreases with increasing initial concentration. As it is obvious, the percentage removal of BTB decreased from around 100% at a concentration of 100 mg/L to 98% when the concentration was increased to 250 mg/L. This behavior reveals the dependency of adsorption to initial concentration of BTB.

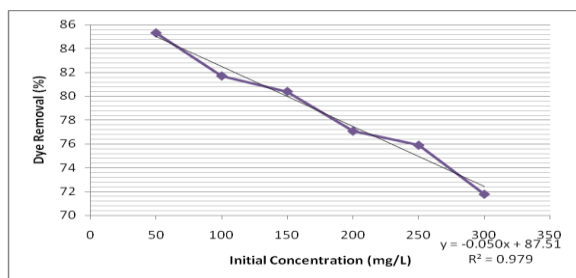


**Fig. 10.** Langmuir isotherm plot of EBT adsorption onto LSCO nanoparticles: LSCO dosage=0.005 g, initial pH= 2, stirring time=15 min, initial dye concentration=100, 150, 200, 250, 300 mg/L.

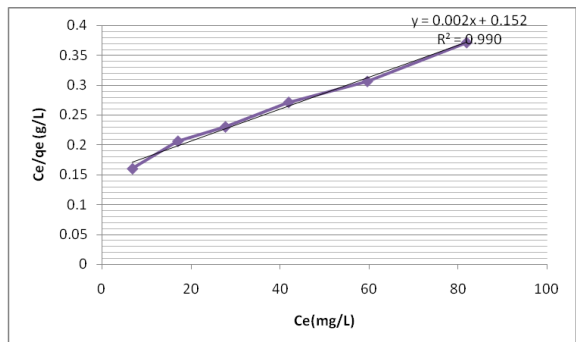


**Fig. 11.** Freundlich isotherm plot of EBT adsorption onto LSCO nanoparticles: LSCO dosage=0.005 g, initial pH= 2, stirring time=15 min, initial dye concentration=100, 150, 200, 250 ,300 mg/L.

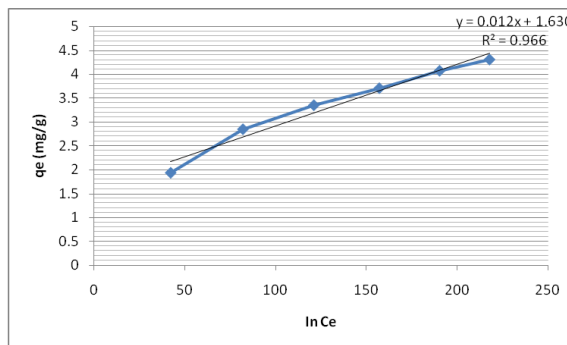


**Fig. 12.** Temkin isotherm plot of BTB adsorption onto LSCO nanoparticles: LSCO dosage=0.01 g, initial pH 2, stirring time=15 min, initial dye concentration=100, 150, 200, 250, 300 mg/L.

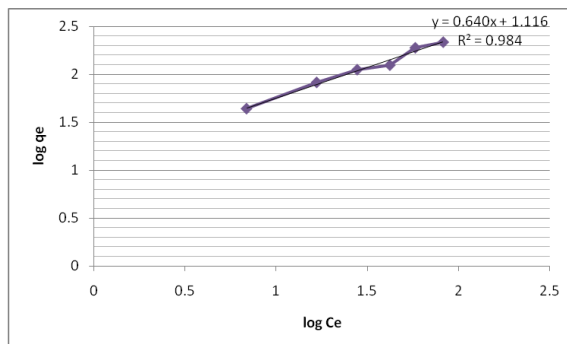


**Fig. 13.** Freundlich isotherm plot of BTB adsorption onto LSCO nanoparticles: LSCO dosage=0.01 g, initial pH 2, stirring time=15 min, initial dye concentration=100, 150, 200, 250, 300 mg/L.

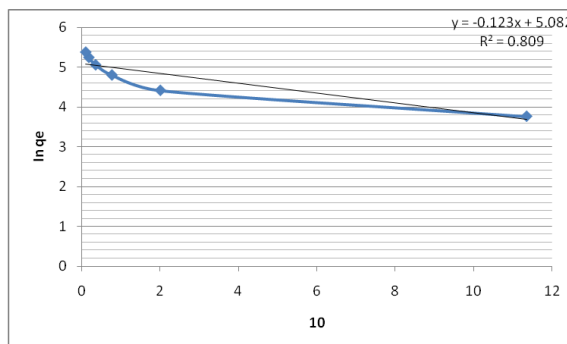


**Fig. 14.** Dubinin-Radushkevich isotherm plot of BTB adsorption onto LSCO nanoparticles: LSCO dosage=0.01 g, initial pH 2, stirring time=15 min, initial dye concentration=100, 150, 200, 250, 300 mg/L.

*Adsorption kinetics*

Several models are available to investigate the adsorption kinetics. The first (Eq. (3)) and second

(Eq. (4)) order reaction rate equations are the most commonly applied models. To find a suitable chemical removal model for describing the experimental kinetic data, the data were fitted into the first and second-order models:

$$\ln C(t) = \ln C_o - k_1 t \quad (3)$$

$$\frac{1}{C(t)} = k_2 t + \frac{1}{C_o} \quad (4)$$

Where  $k_1$  and  $k_2$  are the first-order and second-order rate constants, respectively. The plots of experimental results of the two models showed that the removal of dye follows first-order kinetics with rate constant of  $0.102 \text{ M}^{-1} \text{ min}^{-1}$ .

#### Adsorption isotherms

Analysis of the equilibrium data is important to develop an equation which accurately represents the results and which could be used for design purposes. The results obtained for adsorption of BTB were analyzed by the use of well known models given by the Langmuir, Freundlich, Temkin and Dubinin–Radushkevich, isotherm models (Langmuir, 1918; Freundlich, 1906; Tan *et al.*, 2007; Dubinin *et al.*, 1947). For the sorption isotherms, initial BTB concentration was varied whereas solution pH and amount of adsorbent were held constant. The sorption isotherms for BTB were obtained for LSCO at the solution pH of 2.

$$\frac{C_e}{q_e} = \frac{1}{K_L q_{M_{max}}} + \frac{C_e}{q_{M_{max}}} \quad \text{Langmuir model}$$

$$\log q_e = \log K_F + \frac{1}{n} \log C_e \quad \text{Freundlich model}$$

$$q_e = B \ln K_T + B \ln C_e \quad \text{Temkin model}$$

$$\ln q_e = \ln q_{max} - \beta \epsilon^2 \quad \text{R-D model}$$

where  $C_e$  is the BTB concentration in the solution (mg/L),  $q_e$  is the BTB concentrations in the solid adsorbent (mg/g),  $q_m$  is the maximum adsorption capacity (mg/g),  $K_F$  is a constant related to the adsorption capacity ( $\text{mg}^{1-1/n} \text{ L}^{1/n}/\text{g}$ ),  $b$  is a constant related to the energy of adsorption (L/g),  $n$  is a constant related to the energy of adsorption,  $a$  (L/g) is Temkin constant representing adsorbent–adsorbate interactions and  $b$  ( $\text{mg L}^{-1}$ ) is another constant

related with adsorption heat,  $e$  is the Polanyi potential ( $\text{kJ}^2 \text{ mol}^2$ ) and  $E$  (kJ/mol) is the mean adsorption energy.

To optimize the design of an adsorption system, it is important to establish the most appropriate isotherm model. The correlation factors  $R$  (0.990, 0.9840, 0.8090, 0.9660- for Langmuir, Freundlich, Dubinin–Radushkevich and Temkin models, respectively) confirm good agreement between both theoretical models and our experimental results. The  $R^2$  values for the Langmuir model are closer to unity than those for the other isotherm models for LSCO ( $R^2 = 0.990$ ). The Langmuir isotherm equation is therefore expected to best represent the equilibrium adsorption data. It is clear that the Langmuir isotherm is best fitted for the sorption of BTB LSCO. So, we conclude that the adsorption process may be a homogeneous monolayer adsorption.

#### Conclusions

The nanoprovskite  $\text{La}_{0.5}\text{Sr}_{0.5}\text{CoO}_3$  was prepared by hydrothermal method using citric acid. The XRD reveals that the nanoparticles prepared by calcinating the gel precursor at  $700 \text{ }^\circ\text{C}$  for 4 h have good crystallinity with fine Hexagonal provskite structure. The FTIR spectroscopy confirmed the structure of obtained nanoprovskites. In the present study, we demonstrated the nanoprovskites can act as novel adsorbent materials for degradation of azo dye BTB. The results demonstrated that the BTB dye can be successfully removed from aqueous solutions by the nanoprovskites. A first-order model describes the adsorption kinetic data. The equilibrium adsorption can be described using Langmuir model. In summary, these nanoprovskites are promising candidates for the adsorption of azo dyes from wastewaters.

#### References

Ahmad M, Rahman N. 2011. Equilibrium, kinetics and thermodynamic of remazol brilliant orange 3R dye adsorption on coffee husk-based activated carbon. Chem. Eng. J **170**, 154-161.

- Al-Degs Y, El-Barghouthi M, El-Sheikh A, Walker G.** 2008. Effect of solution pH, ionic strength, and temperature on adsorption behavior of reactive dyes on activated carbon. *Dyes and Pigments* **77**, 16-23.
- Arana J, Herrera Melian J, Dona Rodríguez J, Gonzalez Diaz O, Viera A, Perez Pena J, Marrero Sosa P, Espino Jimenez V.** 2002. TiO<sub>2</sub> photocatalysis as tertiary treatment of naturally treated wastewater. *Catal. Today* **76**, 279-289.
- Bonel G.** 1972. *Annales Chimie* **7**, 127-144.
- Boyer B, Cardoso N, Lima E, Macedo T.** 2010. A useful organofunctionalized layered silicate for textile dye removal. *J. Hazard. Mater* **181**, 366-374.
- Choy K, McKay G, Porter J.** 1999. Sorption of acid dyes from effluents using activated carbon, *Resour. Conserv. Rec* **27**, 57-71.
- Chung K, Stevens S.** 1993. Degradation of azo dyes by environmental microorganisms and helminthes. *Environ. Toxicol. Chem* **12**, 2121-2132.
- Da Silva L, Ruggiero R, Gontijo P, Pinto R, Royer B, Lima E, Fernandes T, Calvete T.** 2011. Adsorption of brilliant red 2BE dye from water solutions by chemically modified sugarcane bagasse lignin. *Chem. Eng. J* **168**, 620-628.
- El Boujaady H, El Rhilassi A, Ziatni M, El Hamri R, Taitai A, Lacout J.** 2011. Removal of a textile dye by adsorption on synthetic calcium phosphates. *Desalination*, in press.
- Eng H, Barnes P, Auer B, Woodward P.** 2003. Investigations of the electronic structure of d transition metal oxides belonging to the perovskite family. *J. Solid State Chem* **175**, 94-109.
- Errais E, Duplay J, Darragi F, M'Rabet I, Aubert A, Huber F, Morvan G.** 2001. Efficient anionic dye adsorption on natural untreated clay: Kinetic study and thermodynamic parameters. *Desalination* **275**, 74-81.
- Forgacs E, Cserhati T, Oros G.** 2004. Removal of synthetic dyes from wastewaters: a review. *Environ. Int* **30**, 953-971.
- Freundlich H.** 1906. Über die adsorption in lasugen. *Z. Phys. Chem* **57A**, 385-470.
- Garcia De La Cruz R, Falcon H, Pena M, Fierro J.** 2001. Role of bulk and surface structures of La<sub>1-x</sub>Sr<sub>x</sub>NiO<sub>3</sub> perovskite-type oxides in methane combustion. *Appl. Catal. B: Environ* **33**, 45-55.
- Gil A, Assis F, Albeniz S, Korili A.** 2011. Removal of dyes from wastewaters by adsorption on pillared clays. *Chem. Eng. J* **168**, 1032-1040.
- Giles C, Macewan T, Smith D.** 1960. Studies in adsorption. Part XI. A system of classification of solution adsorption isotherms, and its use in diagnosis of adsorption mechanisms and in measurement of specific surface areas of solids. *Chem. Soc* **XI**, 3973-3993.
- Hao Y, Li J, Yang X, Wang X, Lu L.** 2004. Preparation of ZrO<sub>2</sub>-Al<sub>2</sub>O<sub>3</sub> composite membranes by sol-gel process and their characterization. *Mater. Sci. Eng. A* **367**, 243-247.
- Hsueh C, Lu Y, Hung C, Huang Y, Chen C.** 2007. Adsorption kinetic, thermodynamic and desorption studies of Reactive Black 5 on a novel photoassisted Fenton catalyst. *Dyes Pigm* **75**, 130-135.
- Indra D, Vimal C, Nitin K.** 2006. Removal of Orange-G and Methyl Violet dyes by adsorption onto bagasse fly ash- kinetic study and equilibrium isotherm analyses. *Dyes Pigm* **69**, 210-223.
- Kao C, Jeng C.** 1999. Preparation and characterization of lanthanum nickel oxides by

combined coprecipitation and molten salt reactions. *Ceram. Int* **25**, 375–382.

**Kao C, Jeng C.** 2000. Preparation and characterisation of lanthanum nickel strontium oxides by combined coprecipitation and molten salt reactions. *Ceram. Int* **26**, 237–243.

**Kim J, Honma I.** 2004. Synthesis and proton conducting properties of zirconia bridged hydrocarbon/phosphotungstic acid hybrid materials. *Electrochim. Acta* **49**, 3179–3183.

**Kritikos D, Xekoukoulotakis N, Psillakis E, Mantzavinos D.** 2007. Photocatalytic degradation of reactive black 5 in aqueous solutions: Effect of operating conditions and coupling with ultrasound irradiation. *Water Res* **41**, 2236–2246.

**Kuznetsov P, Kuznetzova L, Zhyzhaev A, Pashkov G, Boldyrev V.** 2002. Ultra fast synthesis of metastable tetragonal zirconia by means of mechanochemical activation. *Appl. Catal. A* **227**, 299–307.

**Langmuir I.** 1906. The adsorption of gases on plane surfaces. *Phys. Chem. A* **57**, 385–471.

**Leite E, Sousa C, Longo E, Varela J.** 1995. Influence of polymerization on the synthesis of SrTiO<sub>3</sub>: Part I. Characteristics of the polymeric precursors and their thermal decomposition. *Ceram. Int* **21**, 143–152.

**Lin S, Chen M.** 1997. Treatment of textile wastewater by chemical methods for reuse. *Water Res* **31**, 868–876.

**Liu S, Qian X, Xiao J.** 2007. Synthesis and characterization of La<sub>0.8</sub>Sr<sub>0.2</sub>Co<sub>0.5</sub>Fe<sub>0.5</sub>O<sub>3±δ</sub> nanopowders by microwave assisted sol–gel route. *J. Sol-Gel Sci. Technol* **44**, 187–193.

**Mansilla H, Bravo C, Ferreyra R, Litter M, Jardim W, Lizama C, Freer J, Fernandez J.** 2006. Photocatalytic EDTA degradation on suspended and immobilized TiO<sub>2</sub>. *J. Photochem. Photobiol. A. Chem* **181**, 188–194.

**Mazloumia M, Shahcheraghia N, Kajbafvala A, Zanganeha S, Laka A, Mohajerania M, Sadrnezhaad S.** 2009. 3D bundles of self-assembled lanthanum hydroxide nanorods via a rapid microwave-assisted route. *J. Alloys Compd* **473**, 283–287.

**Meadowcroft D.** 1970. Low-cost Oxygen Electrode Material. *Nature* **226**, 847–848.

**Neumann A, Walter D.** 2006. The thermal transformation from lanthanum hydroxide to lanthanum hydroxide oxide. *Thermochim. Acta* **445**, 200–204.

**Nimmo W, Ali N, Brydson R, Calvert C, Hampartsoumian E, Hind D, Milne S.** 2003. Formation of lead zirconate titanate powders by spray pyrolysis. *J. Am. Ceram. Soc* **86**, 1474–1480.

**Oliveira D, Carneiro P, Sakagami M, Zanoni M, Umbuzeiro G.** 2007. Chemical characterization of a dye processing plant effluent- Identification of the mutagenic components. *Mutat. Res* **626**, 135–142.

**Pantelis A, Nikolaos P, Dionissios M.** 2006. Treatment of textile dyehouse wastewater by TiO<sub>2</sub> photocatalysis. *Water Res* **40**, 1276–1286.

**Robinson T, McMullan G, Marchant R, Nigam P.** 2001. Remediation of dyes in textile effluent: a critical review on current treatment technologies with a proposed alternative. *Bioresour. Technol* **77**, 247–255.

- Sakar-Deliormanl A, Celik E, Polat M.** 2009. Solubility and aging of lead magnesium niobate in water. *Ceram. Int* **35**, 503–508.
- Singh R, Lal B.** 2000. High surface area lanthanum cobaltate and its A and B sites substituted derivatives for electrocatalysis of O<sub>2</sub> evolution in alkaline solution. *Int. J. Hydrogen Energy* **27**, 45–55.
- Tanabe K.** 2003. Catalytic application of niobium compounds. *Catal. Today* **78**, 65–77.
- Van der Zee F, Bouwman R, Strik D, Lettinga G, Field J.** 2001. Application of redox mediators to accelerate the transformation of reactive azo dyes in anaerobic bioreactors. *Biotechnol. Bioeng* **75**, 691–701.
- Van der Zee F, Villaverde S.** 2005. Combined anaerobic–aerobic treatment of azo dyes- A short review of bioreactor studies. *Water Res* **39**, 1425–1440.
- Vandevivere P, Bianchi R, Verstraete W.** 1998. Treatment and reuse of wastewater from the textile wet-processing industry: Review of emerging technologies. *J. Chem. Technol. Biotechnol* **72**, 289–302.
- Weisburger J.** 2002. Comments on the history and importance of aromatic and heterocyclic amines in public health. *Mutat. Res* **506**, 9–20.
- Yazdanbakhsh M, Tavakkoli H, Hosseini S.** 2011. Characterization and evaluation catalytic efficiency of La<sub>0.5</sub>Ca<sub>0.5</sub>NiO<sub>3</sub> nanopowders in removal of reactive blue 5 from aqueous solution. *Desalination* **281**, 388–395.
- Yongfa Z, Ruiqin T, Tao Y, Song G, Chunhua Y, Lili C.** 2000. Preparation of nanosized La<sub>2</sub>CuO<sub>4</sub> perovskite oxide using an amorphous heteronuclear complex as a precursor at low-temperature. *J. Alloys and Comp* **311**, 16– 21.